Journal of Materials Processing Technology 213 (2013) 759–769

Contents lists available at SciVerse ScienceDirect

Journal of Materials Processing Technology

journal homepage: www.elsevier.com/locate/jmatprotec

A new method for predicting Forming Limit Curves from mechanical properties

Michael Abspoel*, Marc E. Scholting, John M.M. Droog

Tata Steel Research Development & Technology, Netherlands

ARTICLE INFO

Article history:
Received 15 August 2012
Received in revised form 24 October 2012
Accepted 24 November 2012
Available online 3 December 2012

Keywords:
Forming Limit Curve
Stamping
Sheet metal

ABSTRACT

Forming Limit Curves (FLCs) are an important tool in steel sheet metal forming. Experimental measurements of FLCs are costly, and therefore, empirical prediction methods are of practical use. Difficulties in accurately defining FLCs for new steel grades, such as AHSS, have necessitated a review of the existing prediction methods. Four points were defined to characterise an FLC, and correlations between the coordinates of these points and the mechanical properties from tensile testing were found. The results show that the total elongation, Lankford coefficient and thickness are strongly related to the FLC values. Predictive equations were derived from the statistical relations between the measured FLC points and the mechanical properties. To verify the predictive equations, predicted FLCs for approximately fifty steel grades in various thickness ranges were compared with measured FLCs. It was found that the newly developed method accurately predicts the FLCs.

1. Introduction

Forming Limit Curves (FLCs) are an important tool in Finite Element stamping simulations and in practical press shop investigations because they provide a measure of the failure risk. However, the experimental determination of FLCs requires linear strain paths and is time-consuming, and the scatter in the resulting FLCs is large. Therefore, empirical methods based on calculating the FLC from tensile test data have been popular for many decades.

Keeler and Brazier (1977) proposed a standard-shaped curve that separates major–minor strain points for safe areas from those for areas in which there is necking. The minimum of the curve, FLC_0, is at the plane strain axis, and it increases with increases in the work hardening exponent and increasing sheet thicknesses. They also found that above a certain sheet thickness, the dependence on thickness levels off. Raghavan et al. (1992) described a slightly different curve and gave an equation for positioning the curve along the vertical axis in which FLC_0 increases with increasing total elongation and sheet thickness. Shi and Gelisse (2006) reported that the empirical Keeler equation is still the method of choice in press shops in North America.

Cayssials (1998) developed an approach that was based on damage theories and reported that the key influencing parameters are the strain rate sensitivity, the strain hardening and the sheet thickness. He also compared the FLC_0 predictions of his model with Keeler model predictions and with experimental values. The comparison showed that the Keeler model was only reliable for classical forming-grade steels. The work was extended by Cayssials and Lemoine (2005), who reported that they had developed a model that predicted the FLC from the measured parameters from uniaxial tensile tests: ultimate tensile strength, uniform elongation, the Lankford coefficient and the thickness of the steel. Their papers do not provide equations that make it possible to calculate the FLC, and the only way to obtain a Cayssials-FLC is through AutoForm Finite Element simulation software. Chinouilh et al. (2007) adapted the Cayssials-type prediction with a formalism for stainless steels. From their paper, it becomes clear that the Cayssials-type FLC is determined by four points, the lowest point being on the plane strain axis. Cayssials (1998) also described a critical thickness above which the FLCs become independent of the sheet thickness.

Gerlach et al. (2010a,b) analysed a large set of FLCs measured with Nakazima tests. They fitted the experimental points that define the Forming Limit Curves with a linear function for the left-hand side and an exponential function for the right-hand side. They defined three points, the plane strain point $\varepsilon_1(0)$, the curve minimum $\varepsilon_1(\varepsilon_0)$ and the major strain at minor strain 0.2, called $\varepsilon_1(0.2)$, and provided equations to calculate these three characteristic points based on three parameters from tensile tests: tensile strength, total elongation and sheet thickness. The predicted FLC has a minimum to the right of the plane strain axis, as is usually observed in FLCs measured with the Nakazima method. Abspoel et al. (2011b) described an approach to predict FLCs from mechanical properties to set up a consistent database of FLCs.

However, Atzema et al. (2002) postulated that the Nakazima test should be corrected for the non-proportional strain path at the start of the test induced by the hemispherical punch (biaxial

* Corresponding author. Tel.: +31 251491735.
E-mail addresses: michael.abspoel@tatasteel.com (M. Abspoel), marc.scholting@tatasteel.com (M.E. Scholting), john.droog@tatasteel.com (J.M.M. Droog).

0924-0136/$ – see front matter © 2012 Elsevier B.V. All rights reserved.
http://dx.doi.org/10.1016/j.jmatprotec.2012.11.022

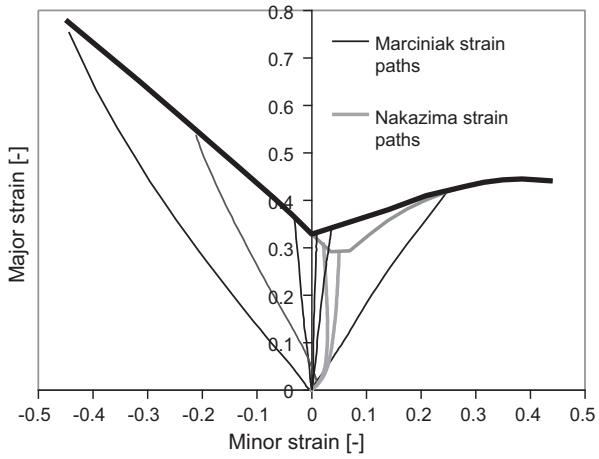

Fig. 1. Comparison of strain paths for Nakazima and Marciniak tests on a forming grade steel. Biaxial pre-strain in the Nakazima test causes a change in the shape of the Forming Limit Curve.

pre-strain). Leppin et al. (2008) and Abspoel et al. (2011a) reported experimental evidence that endorses this. At the end of Nakazima, Marciniak and uniaxial tensile testing there are also (smaller) strain path non-proportionalities which do not cause differences between the Nakazima and Marciniak FLC tests. After the correction of the biaxial pre-strain, FLCs measured with Nakazima tests will show a minimum at plane strain, just as FLCs measured with Marciniak tests do, as is shown in Fig. 1. Therefore, there is a need to review the method to predict FLCs from tensile test data.

Following the findings that the lowest point in the FLC is on the plane strain axis, we have defined four points, shown in Fig. 2, that together provide a practical description of the FLC. Subsequently, for a set of materials covering the range of steel grades and thicknesses that are commercially available, we have searched for relationships between these FLC points and mechanical properties from standard uniaxial tensile testing.

The FLC-uniaxial tensile points were determined from local necking strains measured with on-line optical strain measurement equipment on uniaxial tensile test samples. The three other points (plane strain, intermediate stretch point and equi-biaxial stretch point) were determined from test pieces drawn to failure by either a test with a hemispherical punch as described by Nakazima et al. (1968) or a test with a flat punch as developed by Marciniak and Kuczyński (1967). The uniaxial tensile points showed a strong correlation with the total elongation (A_{80}), the Lankford coefficient

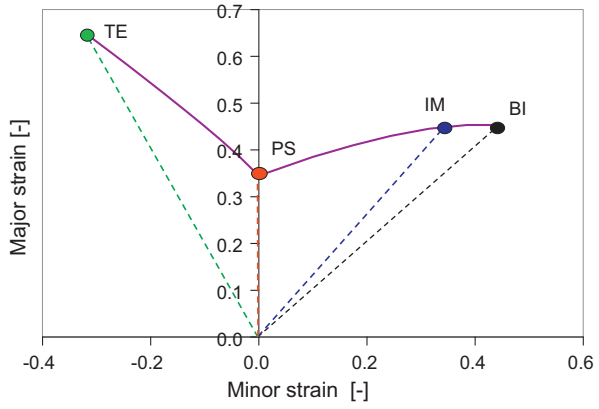

Fig. 2. The four chosen points to define Forming Limit Curves: uniaxial tension necking point (TE), plane strain point (PS), intermediate biaxial stretch point (IM) and equi-biaxial stretch point (BI).

(r value) and the thickness. The three other FLC-points showed a strong correlation with the total elongation and the thickness.

Predictive equations were derived from the statistical relations between the measured FLC points and the mechanical properties. To verify the equations, predicted FLCs for approximately fifty steel grades in various thickness ranges, were compared with measured FLCs.

2. Experimental work

All materials for this investigation were obtained from regular steel production. Fig. 3 shows the range of mechanical properties. The ultimate tensile strengths vary between 280 and 1200 MPa, and the total elongation varies between 5 and 50%. The Lankford coefficients range from 0.6 to 2.7, and the thicknesses range from 0.2 to 3.1 mm.

A wide spectrum of steels was investigated. The materials involved are cold-rolled and hot-rolled forming steels, bake-hardening steels, interstitial free steels, micro-alloyed HSLA steels, direct-rolled structural steels, hot-rolled structural steels, dual-phase steels, TRIP steels, TWIP steels and quenched boron steels.

The mechanical properties were obtained from uniaxial tensile tests, performed according to ISO 6892-1:2009, on Instron-type 5585H or Zwick-type BZ100/SW3A testing equipment. A gauge length of 80 mm was used to determine the total elongation A_{80}. The r-values and the n-values were determined between 2% and 20% strain or between 2% and uniform elongation when the uniform elongation was lower than 20%.

Forming Limit Curve uniaxial tension local necking points were obtained using an MTS 300 test bench with a GOM Aramis optical strain measurement system. The samples were measured transverse to the rolling direction. The other characteristic points were derived from Nakazima and Marciniak tests according to ISO 12004-2: 2008, performed on an Erichsen model 145/60 laboratory press. The samples were measured transverse to the rolling direction. All measured strains in the Nakazima tests were corrected to the mid-plane.

In standard uniaxial tensile tests, the conventional plastic strain ratio is defined as the ratio of the true width strain to the true thickness strain in the measurement area, which is often 20 mm × 80 mm. The upper limit is at the uniform elongation Ag. In the ARAMIS optical measurement we used a grid dimension of 0.3 mm × 0.3 mm to measure local strain evolution over time. Ten Horn et al. (2012) describe how the grid dimensions can be set at a desired value. Fig. 4 shows an example of major and minor strains in an area of later failure. It is clear that after the end of uniform elongation, further strain development concentrates in a small area. It is also clear that the local strain ratio can change over the course of the experiment.

3. Predictive method

3.1. Introduction

The mechanical properties from the tensile testing are the yield strength (Rp), tensile strength (Rm), uniform elongation (Ag), total elongation (A_{80}), hardening exponent (n-value) and strain ratio (r-value). The influence of these mechanical properties on the characteristics of FLCs was studied. Fig. 5 shows the necking strain under plane strain tension plotted vs. several mechanical properties. Rp (Fig. 5a), Rm (Fig. 5b) and the r-value (Fig. 5e) show some correlation with the necking strain. The uniform elongation (Fig. 5c) and the n-value (Fig. 5f) show a linear trend for many steels, but some steels do not follow this trend. These steels are identified as dual-phase steels and TRIP steels. The total elongation (A_{80}) (Fig. 5d)

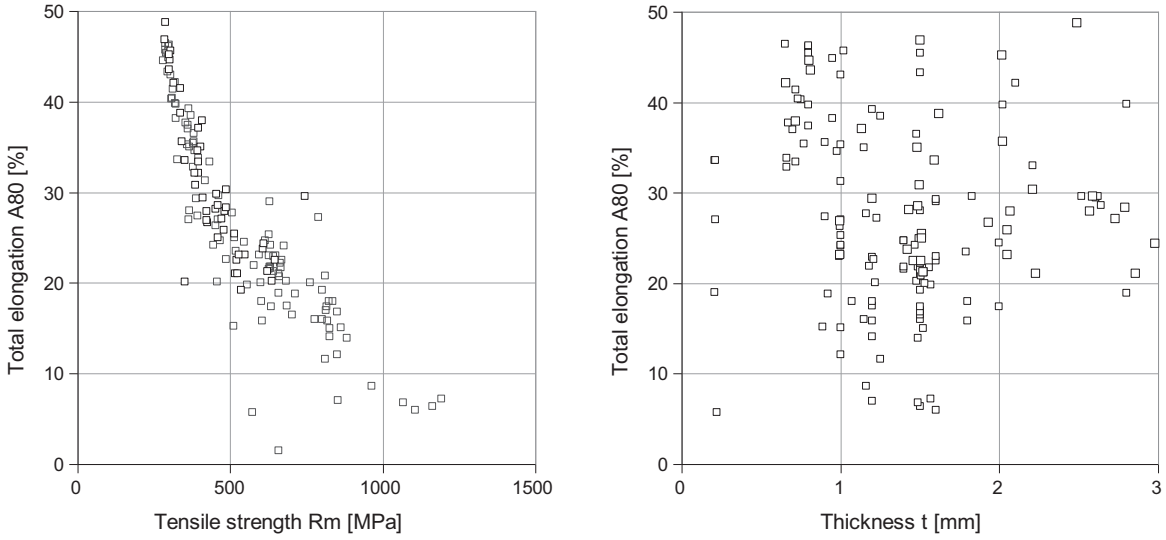

Fig. 3. Overview of all measured steel grades. Left: total elongation vs. tensile strength plotted and right: total elongation vs. thickness.

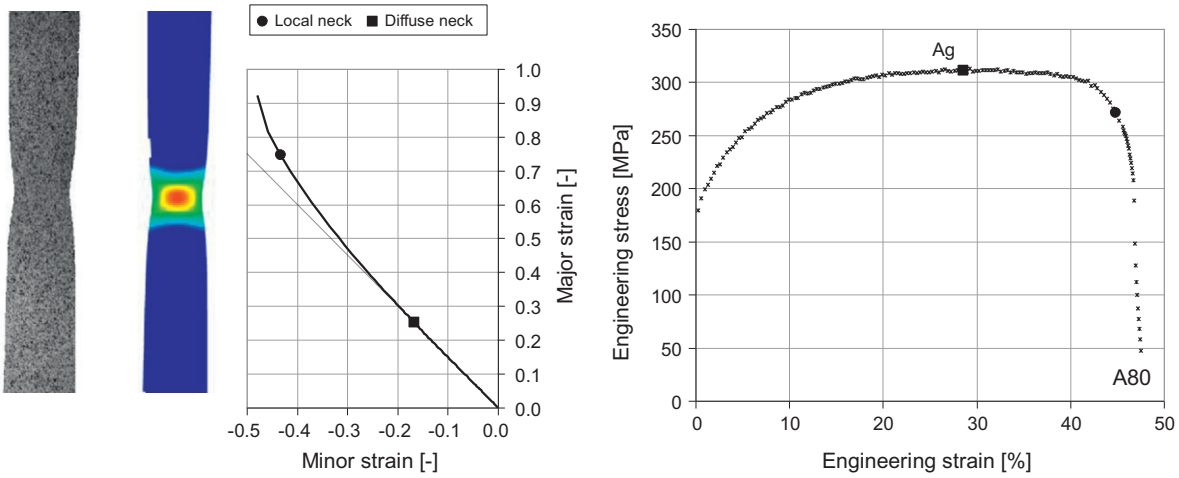

Fig. 4. Local strain development over time in the area of failure (left) and engineering stress–strain curve (right).

Table 1
Notations and definitions for mechanical properties and local strains.

Symbol	Description	Unit
Rm	Tensile strength	MPa
Rp	Yield strength	MPa
Ag	Uniform elongation	%
A_{80}	Total elongation in the direction the FLC is determined	%
A_{80}^{MIN}	Minimum total elongation of transverse, diagonal of longitudinal to rolling	%
r	Lankford value or strain ratio at uniform elongation in the direction the FLC is determined	[–]
ρ	Strain ratio at local necking for uniaxial loading	[–]
t	Thickness	mm
t^{trans}	Transition thickness	mm
SVL	Strain Vector Length (true strain)	[–]
SVL1	Strain Vector Length for 1 mm thick material (true strain)	[–]
ΔSVL	Strain Vector Length increase (true strain)	[–]
C^{dir}	Slope of the Strain Vector Length increase due to thickness	[–]/mm
ε_1^X	True major necking strain	[–]
ε_2^X	True minor necking strain	[–]
ε_3^X	True thickness necking strain	[–]
α	Angle of the FLC between plane strain and uniaxial necking	Degrees
Index X for strains	TE: uniaxial tension condition	
	PS: plane strain tension condition	
	PS1: plane strain tension condition for 1 mm material	
	IM: intermediate biaxial stretching (strain path 0.75)	
	IM1: intermediate biaxial stretching (strain path 0.75) for 1 mm material	
	BI: equi-biaxial stretching condition	
	BI1: equi-biaxial stretching condition for 1 mm material	

Note that A_{80} and the r-value are for the direction the FLC is determined for, but A_{80}^{MIN} is the lowest value for all directions tested.

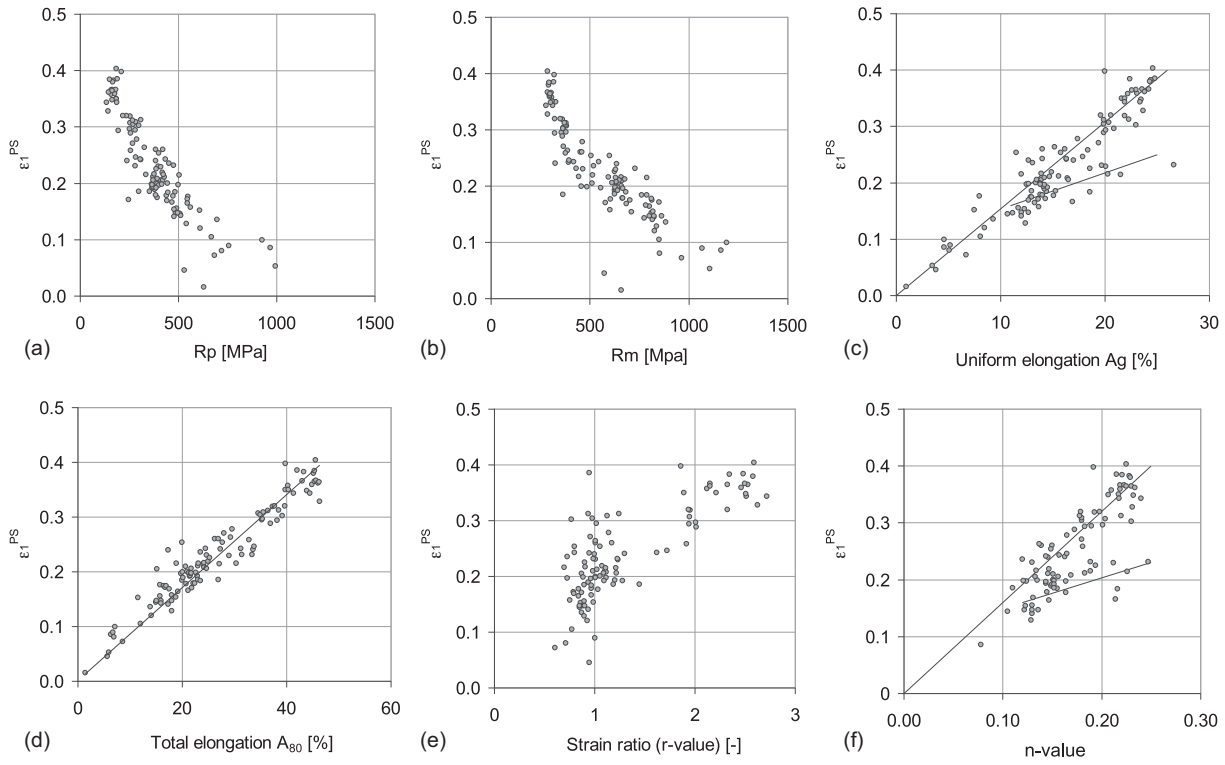

Fig. 5. Relationships between measured necking strains at plane strain and mechanical properties from tensile testing.

shows a good linear correlation. The points that deviate most are identified as materials with the highest or lowest thickness. To obtain a model that is as simple as possible, the total elongation was selected as a parameter for further investigation, along with the thickness. The notations and definitions that are used are given in Table 1.

3.2. Uniaxial tension necking point

From the strain measurements of the tensile samples at the onset of local necking, the local major strain ε_1 and minor strain ε_2 at necking were obtained. From these, the local thickness strain ε_3 at necking was calculated. This local minor strain and the local thickness strain are shown in Fig. 6. Five samples are plotted, from which the effect of increasing A_{80} or the r-value is explained. Each local necking point can be described with a Strain Vector Length (SVL) in the ε_2–ε_3 plane and its local strain ratio at necking (ρ).

$$\mathrm{SVL} = \sqrt{\left(\varepsilon_2^{\mathrm{TE}}\right)^2 + \left(\varepsilon_3^{\mathrm{TE}}\right)^2} \tag{1}$$

$$\rho = \frac{\varepsilon_2^{\mathrm{TE}}}{\varepsilon_3^{\mathrm{TE}}} \tag{2}$$

The examples in Fig. 6 show that an increase in the total elongation increases the Strain Vector Length, but will not change the local strain ratio. For an increasing thickness, a change in the Strain

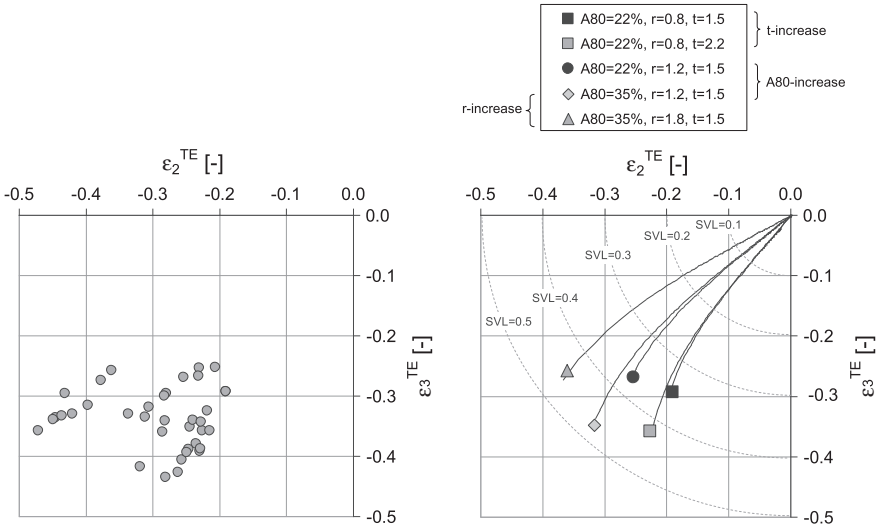

Fig. 6. Left: strains at local necking in uniaxial tensile test experiments. Right: five examples with their strain path history from the start of the tensile test until the onset of local necking.

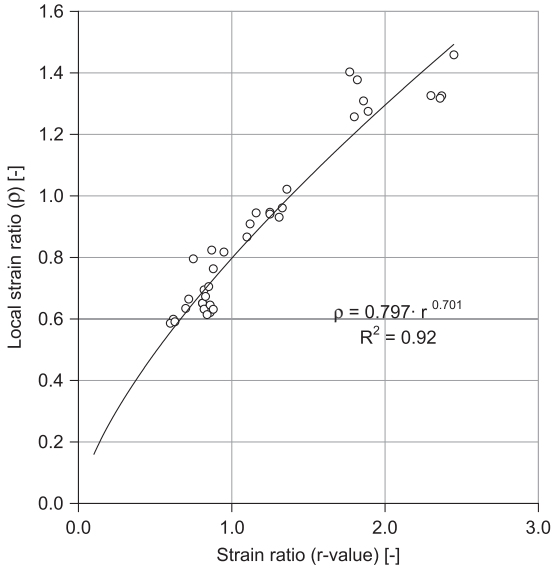

Fig. 7. The local strain ratio (ρ) at necking vs. the strain ratio (r-value) from the tensile test.

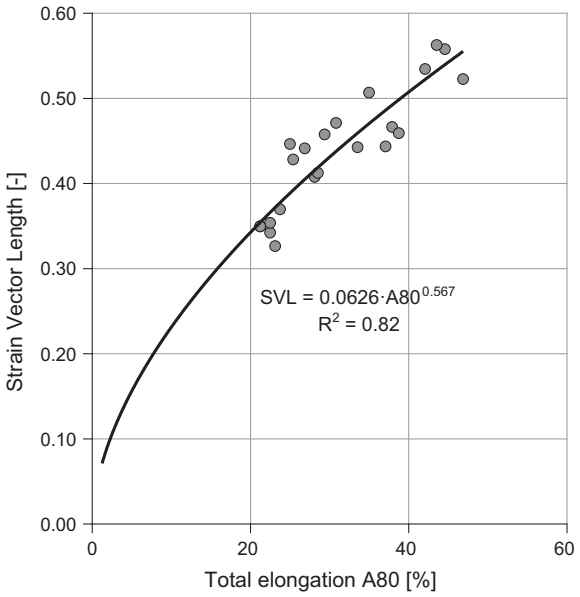

Fig. 8. Strain Vector Length vs. total elongation (A_{80}) for materials between 0.5 and 1.5 mm.

Vector Length is observed. Furthermore, a change in the r-value will change the local strain ratio. We assume the Strain Vector Length can be written as a function of A_{80} and that the thickness and the local strain ratio can be related to the strain ratio at uniform elongation.

$$\rho = f(r) \tag{3}$$

$$\mathrm{SVL} = f(A_{80}, t) \tag{4}$$

With the assumption of constant volume, proportional loading and negligible elasticity, the local strains can be written as:

$$\varepsilon_3^{\mathrm{TE}} = -\sqrt{\frac{\mathrm{SVL}^2}{1+\rho^2}} \tag{5}$$

$$\varepsilon_2^{\mathrm{TE}} = -\rho \cdot \sqrt{\frac{\mathrm{SVL}^2}{1+\rho^2}} \tag{6}$$

$$\varepsilon_1^{\mathrm{TE}} = (1+\rho) \cdot \sqrt{\frac{\mathrm{SVL}^2}{1+\rho^2}} \tag{7}$$

To predict the local strain ratio and the vector length, these properties were correlated with regular mechanical properties. Fig. 7 shows the correlation of the local strain ratio with the r-value. When the r-value is small, the local strain ratio is also small, and therefore, the curve was chosen to go through the origin. The data are not linear, and the simplest non-linear equation, a power law, is chosen. With the final verification, the implication of this choice is verified. The local strain ratio ρ at the onset of necking can be predicted with the strain ratio at uniform elongation, the r-value:

$$\rho = \frac{\varepsilon_2^{\mathrm{TE}}}{\varepsilon_3^{\mathrm{TE}}} = 0.797 \cdot r^{0.701} \tag{8}$$

Fig. 8 shows how the Strain Vector Length correlates with the total elongation A_{80}. Obviously, the strain vector equals zero when the total elongation equals zero. No total elongation means there is no strain and therefore no Strain Vector Length. Additionally, for the Strain Vector Length, the simplest non-linear equation, a power law, is chosen, and the implication is verified with the final validation. Because the Strain Vector Length is also dependent on thickness, only the thinner materials (0.5–1.5 mm) were used for the A_{80} correlation. The relationship found for materials with an average thickness of 1 mm is:

$$\mathrm{SVL1} = 0.0626 \cdot A_{80}^{0.567} \tag{9}$$

To investigate the thickness dependence, the individual Strain Vector Lengths for groups of materials with similar total elongations were plotted vs. the thickness, as shown in Fig. 9. For higher total elongation values, the slope of the thickness dependence decreases. The slope for an individual group is written as:

$$C^{\mathrm{dir}} = \frac{\Delta \mathrm{SVL}}{\Delta t} \tag{10}$$

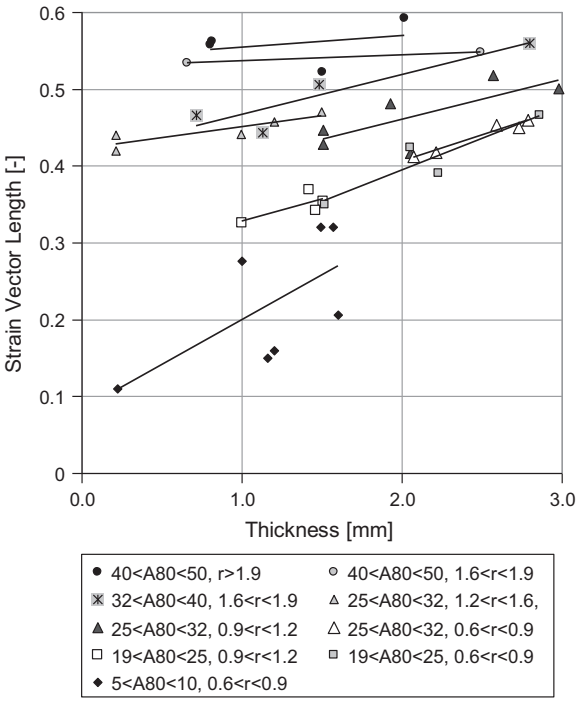

Fig. 9. Strain Vector Length (SVL) vs. thickness per mechanical property group.

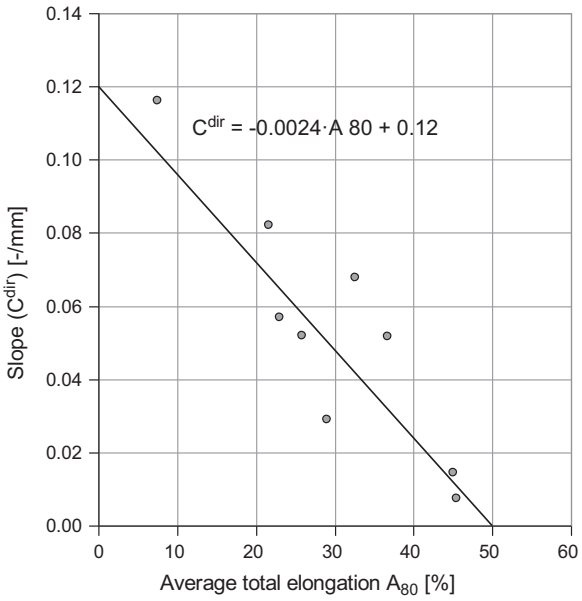

Fig. 10. Thickness dependence slopes of the Strain Vector Length for various mechanical property groups.

All of the individual slopes are plotted in Fig. 10 vs. the average total elongation for the measured samples in the group. Due to the small amount of samples per group, the scatter in the slope is large. A linear trend is chosen, and the implication of this choice is verified with the final validation.

The slope can be described with:

$$C^{\mathrm{dir}} = \frac{\Delta \mathrm{SVL}}{\Delta t} = -0.0024 \cdot A_{80} + 0.12 \tag{11}$$

It follows that the Strain Vector Length increase is dependent on thickness:

$$\Delta \mathrm{SVL} = (-0.0024 \cdot A_{80} + 0.12) \cdot \Delta t \tag{12}$$

Combining (9) and (12), we obtain an equation for the Strain Vector Length:

$$\mathrm{SVL} = \mathrm{SVL1} + \Delta \mathrm{SVL} = 0.0626 \times A_{80}^{0.567} + (t-1) \cdot (0.12 - 0.0024 \cdot A_{80}) \tag{13}$$

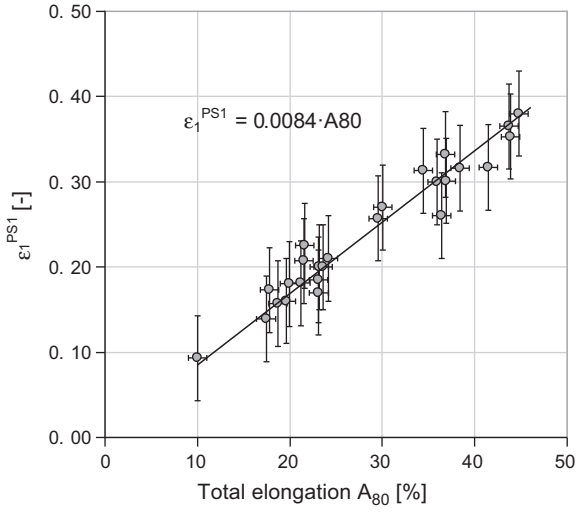

Fig. 11. Necking strain under plane strain tension vs. total elongation A_{80} (materials 1 mm ± 0.2 mm).

By substituting the equations for the local strain ratio ρ and the Strain Vector Length in (5)–(7), the necking strains in the tensile point can be written as:

$$\varepsilon_3^{\mathrm{TE}} = -\frac{(0.0626 \cdot A_{80}^{0.567} + (t-1) \cdot (0.12 - 0.0024 \cdot A_{80}))}{\sqrt{(1 + (0.797 \cdot r^{0.701})^2)}} \tag{14}$$

$$\varepsilon_2^{\mathrm{TE}} = -\frac{(0.0626 \cdot A_{80}^{0.567} + (t-1) \cdot (0.12 - 0.0024 \cdot A_{80})) \cdot 0.797 \cdot r^{0.701}}{\sqrt{(1 + (0.797 \cdot r^{0.701})^2)}} \tag{15}$$

$$\varepsilon_1^{\mathrm{TE}} = (1 + 0.797 \cdot r^{0.701}) \times \frac{(0.0626 \cdot A_{80}^{0.567} + (t-1) \cdot (0.12 - 0.0024 \cdot A_{80}))}{\sqrt{(1 + (0.797 \cdot r^{0.701})^2)}} \tag{16}$$

3.3. Plane strain point

Abspoel et al. (2011b) have reported that the necking strain under plane strain tension has a linear correlation with total elongation, and Fig. 11 shows that this was also found in the present investigation.

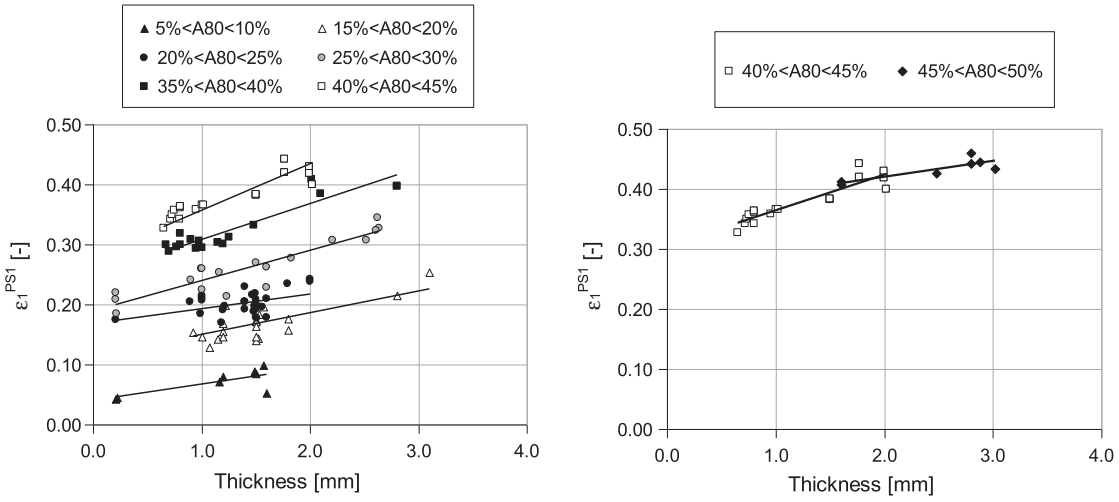

Fig. 12. Plane strain point vs. thickness. Left: six groups used to determine the slope. Right: levelling of the plane strain value for high total elongations.

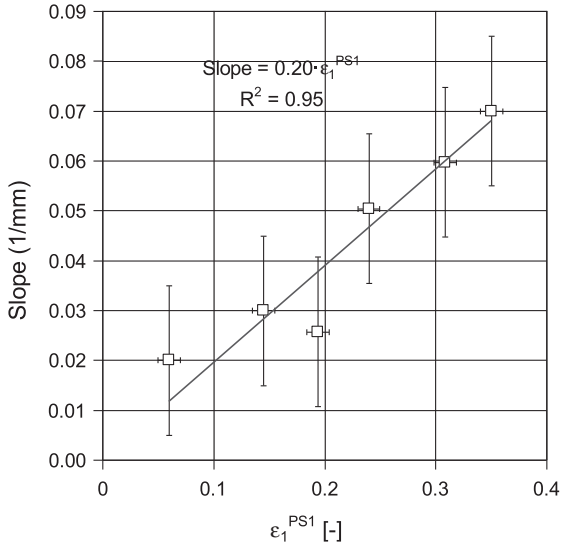

Fig. 13. Thickness dependence slopes of plane strain classes.

The equation derived for 1 mm thick materials is:

$$\varepsilon_1^{PS1} = 0.0084 \cdot A_{80} \tag{17}$$

The thickness dependence of the plane strain point is determined by defining nine groups of similar mechanical properties. The thickness dependencies are shown in Fig. 12.

The slopes for each mechanical property group are now plotted vs. the strain at 1 mm for that group (Fig. 13). There is a linear correlation between the strain and the slope.

For the plane strain point, the increase in strain due to thickness can be written as:

$$\Delta\varepsilon_1^{PS} = 0.20 \cdot \varepsilon_1^{PS1} \cdot (t-1) \tag{18}$$

$$\varepsilon_1^{PS} = \varepsilon_1^{PS1} + \Delta\varepsilon_1^{PS} \tag{19}$$

Combining (17)–(19) leads to the following equation for plane strain:

$$\varepsilon_1^{PS} = 0.0084 \cdot A_{80} + 0.0017 \cdot A_{80} \cdot (t-1) \tag{20}$$

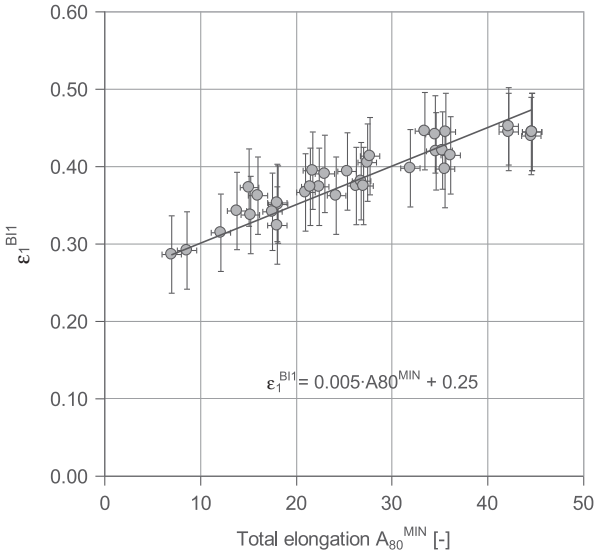

Fig. 14. Equi-biaxial stretching point vs. total elongation A_{80} (materials 1 mm ± 0.2 mm).

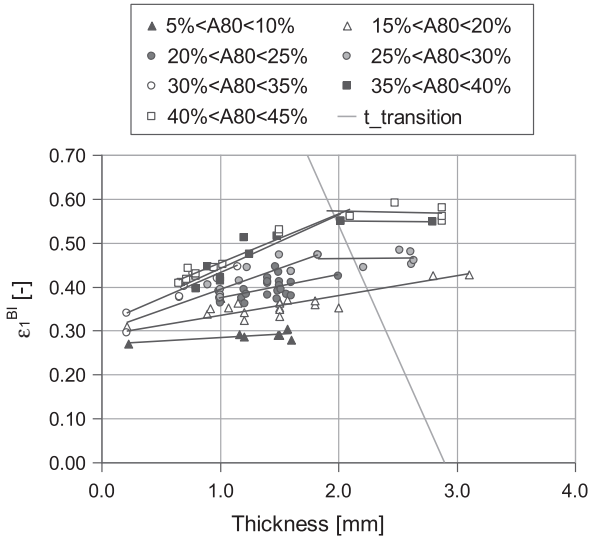

Fig. 15. Equi-biaxial stretching points vs. thickness.

Fig. 12 (right) shows that the maximum plane strain value levels off at a value of 0.45 major strain when the thickness increases for high total elongations.

3.4. Equi-biaxial stretching point

An identical analysis was performed for the equi-biaxial stretching point. In Fig. 14, the biaxial point is plotted vs. the total elongation. The graph shows that there is a linear relation between the two:

$$\varepsilon_1^{BI1} = 0.005 \cdot A_{80}^{MIN} + 0.25 \tag{21}$$

Note that the A_{80} value for the equi-biaxial stretching point must be the minimum value tested from the different directions, 0, 45 or 90° to the rolling direction. This will be the direction with the earliest failure. This anisotropic behaviour is also suggested by Marciniak et al. (1973).

In Fig. 15, the thickness dependence of the equi-biaxial stretching point is determined by defining eight groups of similar mechanical properties. The equi-biaxial stretching point shows an increasing slope for higher total elongations. However, above a

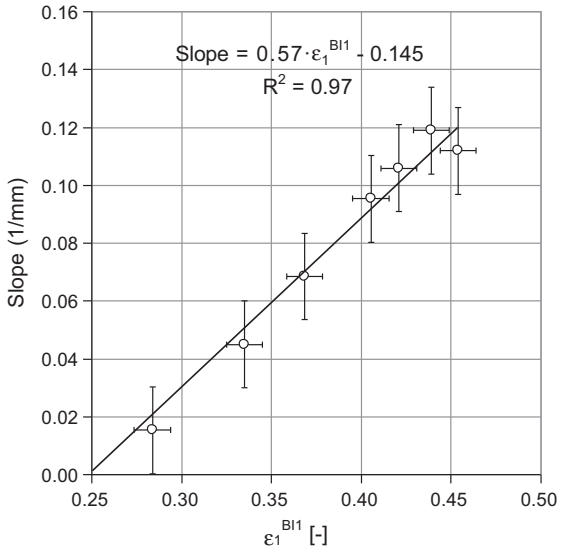

Fig. 16. Thickness dependence slopes of biaxial classes.

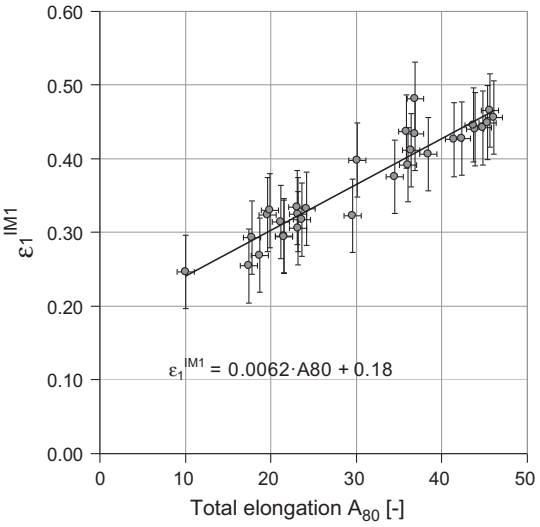

Fig. 17. Intermediate biaxial stretching point vs. total elongation A_{80} (materials 1 mm ± 0.2 mm).

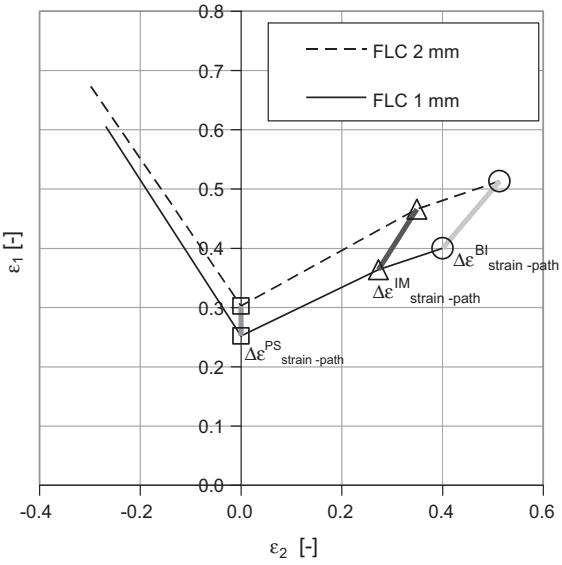

Fig. 18. Scaling the thickness dependence in the strain path.

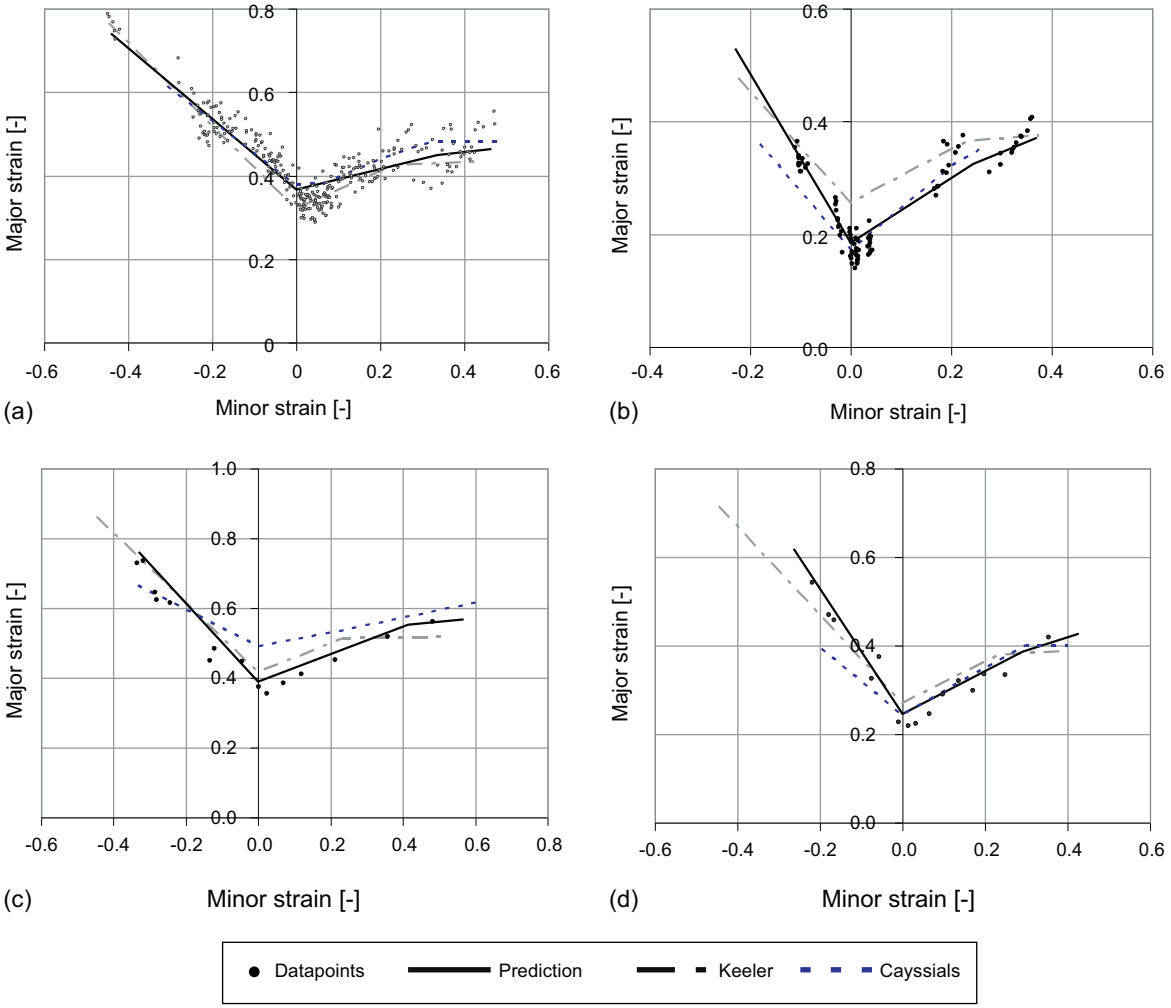

Fig. 19. Examples of predicted FLCs compared with measured (mid-plane) Nakazima FLC points. (a) DC04, multiple coils, A_{80} = 41.5 ± 1.5%, r = 1.9 ± 0.2, t = 1.0 ± 0.2 mm. (b) HCT600X + Z, single coil, A_{80} = 20.7 ± 0.5%, r = 0.99 ± 0.02, t = 1.5 ± 0.01 mm. (c) DD13, single coil, A_{80} = 42.1 ± 0.5%, r = 0.95 ± 0.02, t = 2.1 ± 0.01 mm. (d) S420MC, single coil, A_{80} = 24.0 ± 0.5%, r = 0.80 ± 0.03, t = 2.0 ± 0.01 mm.

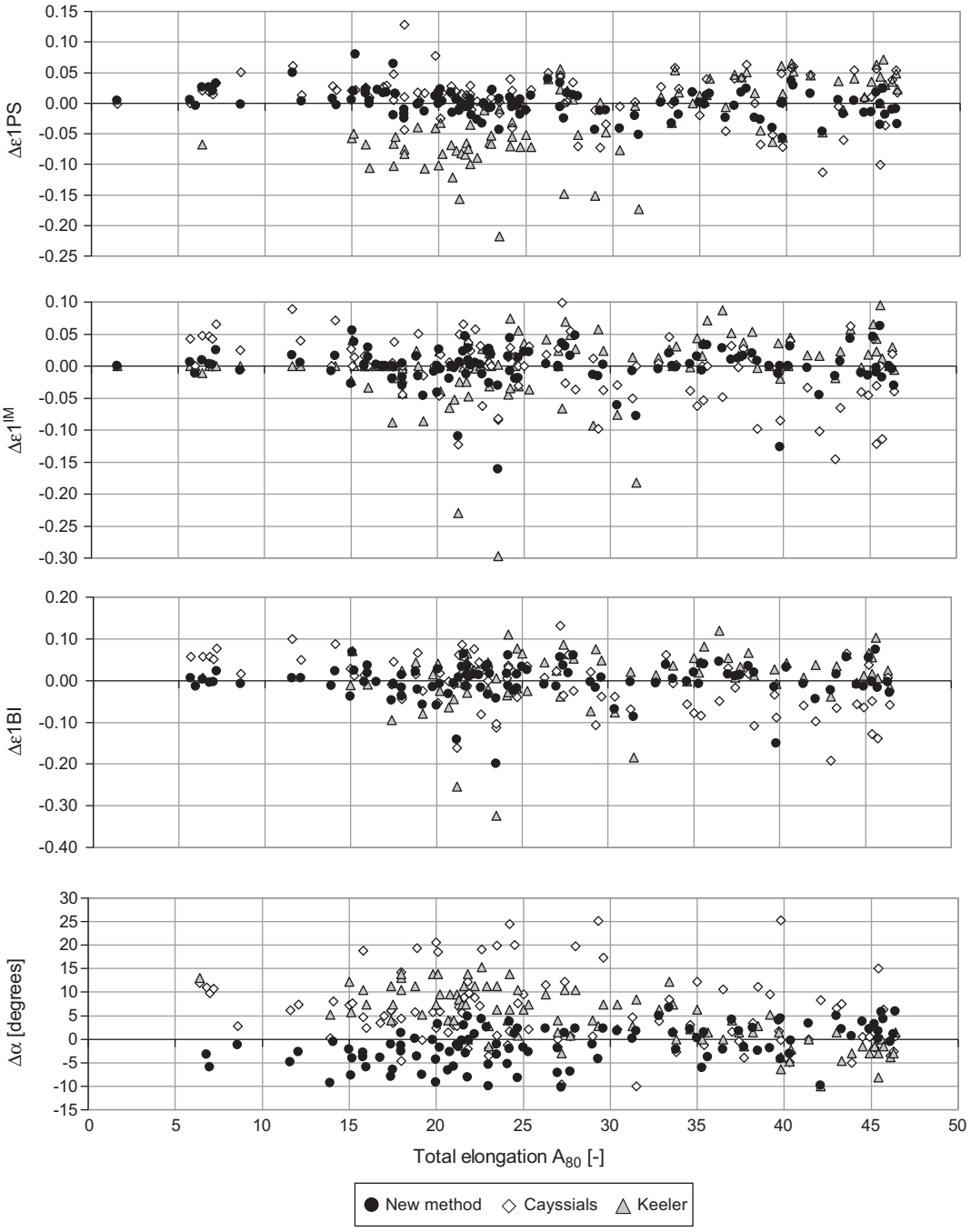

Fig. 20. The upper three graphs show measured major strain values minus predicted values for plane strain points, intermediate points and biaxial points plotted vs. total elongation. The bottom graph shows the same for the slope of the left-hand side of the FLCs.

certain thickness, the strain increase stops. This thickness is called the transition thickness. For the equi-biaxial stretching point, the line of transition is assumed to be:

$$\varepsilon_1^{\mathrm{BI}} = 1.75 - 0.6 \cdot t \tag{22}$$

Now, the slopes for each mechanical property group are plotted vs. the strain at 1 mm for that group (Fig. 16). There is a linear correlation between the strain and the slope.

For the equi-biaxial stretching point, the increase in strain due to thickness can be written as:

$$\Delta\varepsilon_1^{\mathrm{BI}} = 0.57 \cdot \varepsilon_1^{\mathrm{BI1}} \cdot (t - 1) \tag{23}$$

$$\varepsilon_1^{\mathrm{BI}} = \varepsilon_1^{\mathrm{BI1}} + \Delta\varepsilon_1^{\mathrm{BI}} \tag{24}$$

Combining (21), (23) and (24) gives the following for the equi-biaxial stretching point:

$$\varepsilon_1^{\mathrm{BI}} = 0.00215 \cdot A_{80}^{\mathrm{MIN}} + 0.25 + 0.00285 \cdot A_{80}^{\mathrm{MIN}} \cdot t \tag{25}$$

This equation is valid up to the transition thickness. The transition thickness can now be written by combining (22) with (25):

$$t^{\mathrm{trans}} = \frac{1.5 - 0.00215 \cdot A_{80}^{\mathrm{MIN}}}{0.6 + 0.00285 \cdot A_{80}^{\mathrm{MIN}}} \tag{26}$$

Above t^{trans}, the thickness dependence is assumed to be absent.

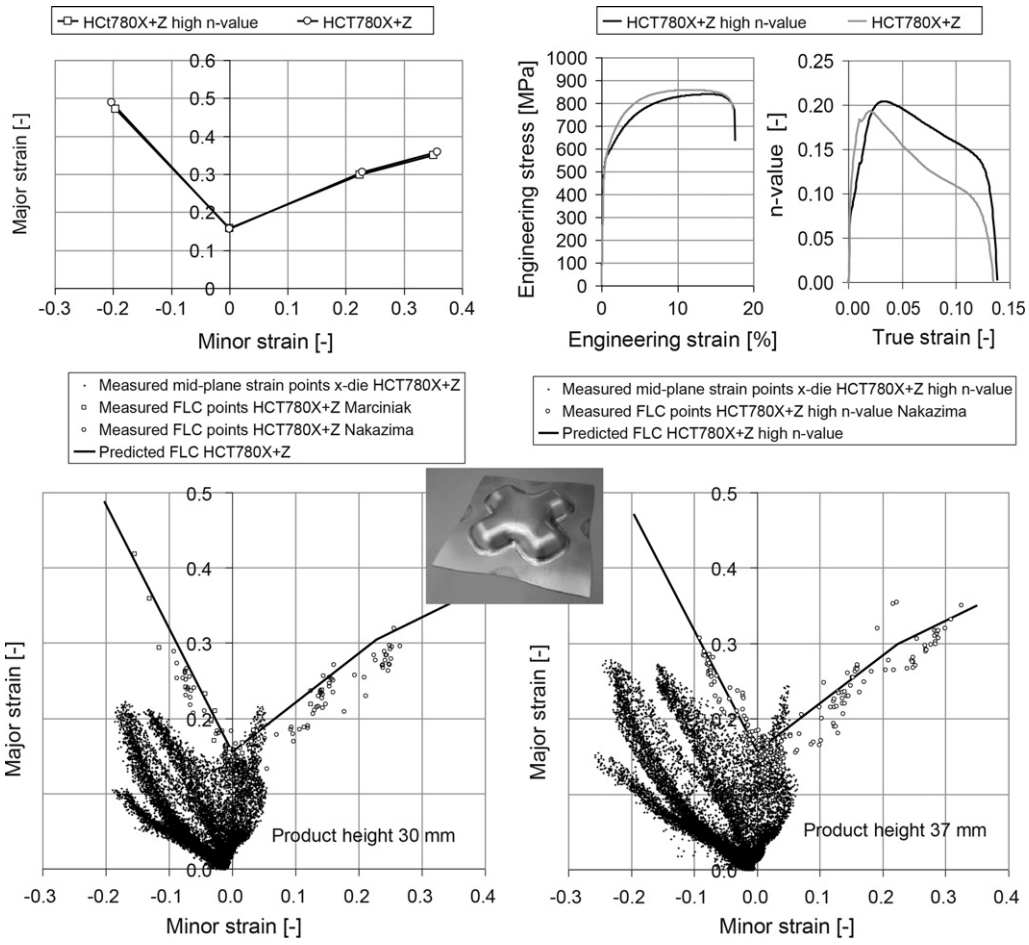

Fig. 21. Comparison of two materials with equivalent predicted and measured FLC but significantly different work hardening behaviour (n-value and Ag). With the high n-value material a higher product can be obtained.

3.5. Intermediate biaxial stretch point (SR 0.75)

The intermediate biaxial stretch points are determined using the intersection of the fitted FLC with the line at a strain ratio of 0.75. In Fig. 17, the intermediate biaxial stretching point is plotted vs. the total elongation. The graph shows a linear relation.

The major strain for materials of 1 mm thickness is:

$$\varepsilon_1^{\mathrm{IM1}} = 0.0062 \cdot A_{80} + 0.18 \tag{27}$$

The thickness dependence for the intermediate biaxial stretching point is scaled in the strain path using the equations for major plane strain and major biaxial major strain thickness dependence, as shown in Fig. 18. For plane strain and biaxial strain, the thickness dependences in the strain path directions are (see Eqs. (20) and (25)):

$$\Delta\varepsilon^{\mathrm{PS}}_{\text{strain-path}} = 0.0017 \cdot A_{80} \cdot t \tag{28}$$

$$\Delta\varepsilon^{\mathrm{BI}}_{\text{Strain-path}} = 0.00285 \cdot A_{80} \cdot t \cdot \sqrt{2} = 0.004 \cdot A_{80} \cdot t \tag{29}$$

For the intermediate biaxial stretch point at a strain ratio of 0.75, the thickness dependence is scaled linearly in the strain path, assuming it is influenced for one quarter by the plane strain and for three quarters by the biaxial point. The implication of this choice is verified in the final validation.

The thickness dependence in the intermediate biaxial stretching point is given by:

$$\Delta\varepsilon^{\mathrm{IM}}_{\text{Strain-path}} = 0.0034 \cdot A_{80} \cdot t \tag{30}$$

Resolving the thickness dependence strain in the major and minor strain direction gives:

$$\Delta\varepsilon_1^{\mathrm{IM}} = 0.0027 \cdot A_{80} \cdot t \rightarrow \varepsilon_1^{\mathrm{IM}} = 0.0062 \cdot A_{80} + 0.18 + 0.0027 \cdot A_{80} \cdot (t-1) \tag{31}$$

$$\varepsilon_2^{\mathrm{IM}} = 0.75 \cdot \varepsilon_1^{\mathrm{IM}} \rightarrow \varepsilon_2^{\mathrm{IM}} = 0.75 \cdot (0.0062 \cdot A_{80} + 0.18 + 0.0027 \cdot A_{80} \cdot (t-1)) \tag{32}$$

When the transition thickness is reached, no more strain increase is assumed, similar to what was done for biaxial strain.

4. Discussion

The equations were verified using a large database of FLCs measured in our laboratory over recent years. The FLC points were obtained with Nakazima or Marciniak tests. For the Nakazima test, the lowest points are located to the right of the minor strain axis. In the predictive method, this test artefact is eliminated. The predictions were also compared with equations for Keeler curves, as described by Shi and Gelisse (2006), and with the Cayssials method, as available in AutoForm plus R3 software (as Arcelor v9 module). Fig. 19 shows four examples. For the cold-rolled forming steel DC04 (Fig. 19a), there is no difference between the new method and the Keeler and Cayssials methods: all predicted FLCs are within the scatter band of the measured points. In contrast, the advanced high-strength steel HCT600X+Z (Dual Phase 600)

(Fig. 19b) shows significant differences. The experimental points support the conclusion of Cayssials (1998) that the Keeler prediction is not satisfactory for these modern steel grades. The slope of the left-hand side of the Cayssials curve deviates from the measured points. In contrast, the left-hand side of our new prediction method agrees better with the measured points. A possible reason for this is the fact that in our method, the *r*-value is taken into account. This directly influences the slope on the left side of the FLC. Fig. 19c shows the results for hot-rolled forming steel DD13. Both the Keeler equations and the new method are in agreement with the measured points. The Cayssials prediction, however, is too high in the plane strain region. Fig. 19d shows that for the high-strength hot-rolled steel S420MC, the best agreement with the measured points is obtained with the new method. Both the Keeler and the Cayssials method predict a too-low slope for the left-hand side of the FLC.

In Fig. 20, all predicted points for all grades investigated are verified. Each predicted major strain is subtracted from its measured major strain. As shown in the examples in Fig. 19, the angle of the left side of the FLC is different for the three prediction methods. This angle is also verified by subtracting the predicted angle from the measured angle. The newly proposed method has a scatter band of ±0.05% true major strain for the three predicted points. The angle scatter band ranges from +5 to −10°, whereas Cayssials and Keeler show a larger scatter band for all measured points and for the angle. For Keeler and Cayssials, especially for the high-strength steels the angle is lower for the predicted than for the measured FLC. The outliers for the new method are identified as TRIP steels. The TRIP steels show a good prediction for the angle and in-plane strain, but the right-hand side is predicted higher than measured. It is possible that the TRIP effect in biaxial tests is not the same in magnitude and in timing as it is in uniaxial tests.

We found that total elongation is a good parameter for predicting the FLC. A possible explanation might be that total elongation is close to local necking as can be seen in Fig. 4. In this way, the effects that occur in the post-uniform elongation trajectory are included. In contrast, the uniform elongation, the tensile strength, yield strength and hardening exponent contain no information about the post-uniform elongation.

Fig. 21 shows the results of press trials with two materials that had equivalent predicted FLCs and similar yield locus, but different work hardening behaviour. The upper part of the figure shows the predicted FLCs, the engineering stress–strain curves and the instantaneous *n*-values vs. true strain. The tensile strain hardening exponent (*n*-value) is usually reported as the average value in a strain range up till 20% or Ag. The lower part of the figure shows the strain distributions on two X-die parts with maximum height. With the high *n*-value material a higher product can be pressed before the material necks, because the material is capable of distributing the strains better.

The level of the FLC-values in all stress states is influenced by the work hardening, both the uniform and post uniform elongation part. The shape of the yield locus influences the right hand side of the FLC as described by Marciniak and Kuczyński (1967). Work hardening is comparable in all stress states. The yield locus connects the work hardening measured under uniaxial stress condition with other stress states.

The reported equations have been tested for steel materials with ultimate tensile strengths between 280 and 1200 MPa, total elongations between 5 and 50%, Lankford coefficients ranging from 0.6 to 2.7, and thicknesses ranging from 0.2 to 3.1 mm.

5. Conclusion

The newly developed method accurately predicts the FLCs for a wide range of steel grades and thicknesses. The FLC can be predicted with the help of mechanical properties A_{80}, the *r*-value and the sheet thickness. The difference in the left-hand side of the FLC between our method and the Cayssials method cannot be investigated in detail because the Cayssials equations are not available in the open literature. The difference with the Keeler method can be explained by the fact that modern steel grades such as AHSS have a different necking behaviour that correlates more to total elongation than to hardening exponent or uniform elongation. AHSSs were not readily available when the Keeler method was being developed.

Acknowledgments

Henk Vegter and Nico Langerak are gratefully acknowledged for stimulating discussions. We thank Tushar Khandeparkar and Frank Schouten for carrying out optical strain measurements and Menno de Bruine for performing the Nakazima and Marciniak tests.

References

Abspoel, M., Atzema, E.H., Droog, J.M.M., Khandeparkar, T., Scholting, M.E., Schouten, F.J., Vegter, H., 2011a. Inherent influence of strain path in Nakazima FLC testing. In: Guttierez, D. (Ed.), Proceedings of 2011 IDDRG Conference. Bilbao, Spain.

Abspoel, M., Atzema, E.H., Droog, J.M.M., Scholting, M.E., 2011b. Setting up a consistent database of FLC's. In: Guttierez, D. (Ed.), Proceedings of 2011 IDDRG Conference. Bilbao, Spain.

Atzema, E.H., Duwel, A., Elliott, L., Neve, P.F., Vegter, H., 2002. Appreciation of the determination of the Forming Limit Curve. In: Yang, D.-Y., Oh, S.I., Huh, H., Kim, Y.H. (Eds.), Proceedings of the Numisheet 2002 Conference. Jeju Island, Korea, pp. 471–476.

Cayssials, F., 1998. A new method for predicting FLC. In: Proceedings of the 20th IDDRG Congress, Brussels, Belgium, pp. 443–454.

Cayssials, F., Lemoine, X., 2005. Predictive model of FLC (Arcelor model) upgraded to UHSS steels. In: Boudeau, N. (Ed.), Proceedings of the 24th International Deep-Drawing Research Group Congress. Besançon, France.

Chinouilh, G., Toscan, F., Santacreu, P.O., Leseux, J., 2007. Forming Limit Diagram Prediction of Stainless Steels Sheets. SAE Technical Paper Serie 2007-01-0338, Michigan, USA, pp. 25–29.

Gerlach, J., Kessler, L., Köhler, A., 2010a. The forming limit curve as a measure of formability—is an increase of testing necessary for robustness simulations? In: Kolleck, R. (Ed.), Proceedings IDDRG 50th Anniversary Conference. , pp. 479–488.

Gerlach, J., Keßler, L., Köhler, A., Paul, U., 2010b. Method for the approximate calculation of forming limit curves using tensile test results. Stahl und Eisen 130, 55–61 (in German).

Keeler., S.P., Brazier, S.G., 1977. Relationship between laboratory material characterization and press-shop formability. In: Proceedings of Microalloying, vol. 75, New York, pp. 517–530.

Leppin, C., Li, J., Daniel, D., 2008. Application of a method to correct the effect of non-proportional strain paths in Nakajima test based forming limit curves. In: Hora, P. (Ed.), Proceedings of Numisheet 2008. Zurich, Switzerland, pp. 217–221.

Marciniak, Z., Kuczyński, K., 1967. Limit strains in the processes of stretch-forming sheet metal. International Journal of Mechanical Sciences 9, 609–620.

Marciniak, Z., Kuczyński, K., Pokora, T., 1973. Influence of the plastic properties of a material on the forming limit diagram for sheet metal in tension. International Journal of Mechanical Sciences 15, 789–805.

Nakazima, K., Kikuma, T., Hasuka, K., 1968. Study on the Formability of Steel Sheets. Yawata Technical Report No. 264, pp. 141–154.

Raghavan, K.S., Van Kuren, R.C., Darlington, H., 1992. Recent Progress in the Development of Forming Limit Curves for Automotive Sheet Steels. SAE Technical Paper 920437.

Shi, M.F., Gelisse, S., 2006. Issues on the AHSS forming limit determination. In: Santos, A.D., Barata de Rocha, A. (Eds.), Proceedings IDDRG International Deep Drawing Research Group 2006 Conference. Porto, Portugal, pp. 19–25.

Ten Horn, C.H.L.J., Khandeparkar, T., Droog, J.M.M., 2012. Improving measurement of strain and strain ratio at fracture in sheet metal forming. In: Proceedings of Werkstoffprüfung, Bad Neuenahr, Germany, pp. 121–126.